5-1-1997

Two-spinon dynamic structure factor of the one-dimensional s=1/2 Heisenberg antiferromagnet

Michael Karbach
University of Rhode Island

Gerhard Müller
University of Rhode Island, gmuller@uri.edu

A. Hamid Bougourzi

Andreas Fledderjohann

Karl-Heinz Mütter

Two-spinon dynamic structure factor of the one-dimensional s=1/2 Heisenberg antiferromagnet

Two-spinon dynamic structure factor of the one-dimensional $s = \frac{1}{2}$ Heisenberg antiferromagnet

Michael Karbach and Gerhard Müller

Department of Physics, The University of Rhode Island, Kingston, Rhode Island 02881-0817

A. Hamid Bougourzi

Institute of Theoretical Physics, SUNY at Stony Brook, Stony Brook, New York 11794

Andreas Fledderjohann and Karl-Heinz Mütter

Physics Department, University of Wuppertal, 42097 Wuppertal, Germany

The exact expression derived by Bougourzi, Couture, and Kacir for the two-spinon contribution to the dynamic spin structure factor $S(q,\omega)$ of the one-dimensional $s=1/2$ Heisenberg antiferromagnet at $T=0$ is evaluated for direct comparison with finite-chain transition rates ($N \leq 28$) and an approximate analytical result previously inferred from finite-N data, sum rules, and Bethe ansatz calculations. The two-spinon excitations account for 72.89% of the total intensity in $S(q,\omega)$. The singularity structure of the exact result is determined analytically and its spectral-weight distribution evaluated numerically over the entire range of the two-spinon continuum. The leading singularities of the frequency-dependent spin autocorrelation function, static spin structure factor, and q dependent susceptibility are determined via sum rules. The impact of the non-two-spinon excitations on the integrated intensity, the susceptibility, the frequency moments, and the Euclidian time representation of $S(q,\omega)$ is studied on the basis of finite-size data. [S0163-1829(97)00517-1]

I. INTRODUCTION

Notwithstanding the fact that Bethe[1] found the key that solves the one-dimensional (1D) $s=1/2$ Heisenberg model,

$$H = J \sum_{l=1}^{N} \mathbf{S}_l \cdot \mathbf{S}_{l+1}, \tag{1.1}$$

as early as 1931, the emergence of explicit results for various physical quantities (ground-state energy,[2] excitation spectrum,[3] magnetization curve, susceptibility,[4] thermodynamics[5]) was slow at first and then faster since around 1960. Interest in this model began to spread far and wide when the first compounds with quasi-1D magnetic properties were synthesized and investigated experimentally.

However, the dynamics of the 1D Heisenberg antiferromagnet ($J>0$) has remained elusive to any rigorous approach during all those years. An exact result for the dynamic spin structure factor

$$S(q,\omega) \equiv \frac{1}{N} \sum_{l,n} e^{iqn} \int_{-\infty}^{+\infty} dt\, e^{i\omega t} \langle S_l^z(t) S_{l+n}^z \rangle, \tag{1.2}$$

in particular, would have been of great value for the interpretation of a host of experimental data.[6]

Significant progress in the understanding of the $T=0$ dynamics resulted from the observation[7] that almost all the spectral weight in $S(q,\omega)$ is carried by a special class of Bethe ansatz solutions with excitation energies (in units of J henceforth)

$$\omega_m(q) = \pi \sin\frac{q}{2} \cos\left(\frac{q}{2} - \frac{q_m}{2}\right), \tag{1.3}$$

$0 \leq q \leq \pi, 0 \leq q_m \leq q$, for $N \to \infty$. In the (q,ω) plane they form a two-parameter continuum bounded by the branches

$$\omega_L(q) = \frac{\pi}{2}\sin q, \quad \omega_U(q) = \pi\sin\frac{q}{2}. \tag{1.4}$$

These excitations were later named *two-spinon* states. Their density of states (rescaled by $2\pi/N$) is[7]

$$D(q,\omega) = \frac{\Theta(\omega - \omega_L(q))\Theta(\omega_U(q) - \omega)}{\sqrt{\omega_U^2(q) - \omega^2}}. \tag{1.5}$$

The $T=0$ dynamic spin structure factor for a finite system with even N and periodic boundary conditions can be written in the form

$$S(q,\omega) = 2\pi \sum_{\lambda} M_\lambda \delta(\omega - \omega_\lambda), \tag{1.6}$$

where $M_\lambda = |\langle G|S_q^z|\lambda\rangle|^2$ with $S_q^z = N^{-1/2}\sum_l e^{iql}S_l^z$ are the transition rates between the singlet ($S_T = 0$) ground state $|G\rangle$ and the triplet ($S_T = 1$) states $|\lambda\rangle$ with finite-N excitation energies ω_λ. Among them are the $N(N+2)/8$ two-spinon excitations, which contribute most of the spectral weight.

The finite-chain analysis of Ref. 7 suggested that the scaled transition rates NM_λ vary smoothly with q and ω. The consequence could be that the exact two-spinon part of $S(q,\omega)$ is expressible, for $N \to \infty$, as a product

$$S^{(2)}(q,\omega) = M(q,\omega)D(q,\omega), \tag{1.7}$$

with a smooth transition-rate function $M(q,\omega)$, toward which the scaled finite-N transition rates converge. This scenario is indeed realized in the related XX model,[8] where the

two-spinon density of states is given by Eq. (1.5) with modified spectral boundaries, and the transition-rate function is a constant.[7]

II. TWO-SPINON TRANSITION RATES

In the Heisenberg model (1.1), the finite-N data for the two-spinon matrix elements indicate that $M(q,\omega)$ diverges at $\omega=\omega_L(q)$ and vanishes at $\omega=\omega_U(q)$. In Ref. 7 the expression

$$M^{(a)}(q,\omega)=\sqrt{\frac{\omega_U^2(q)-\omega^2}{\omega^2-\omega_L^2(q)}} \qquad (2.1)$$

for the two-spinon transition-rate function was proposed on the basis of this observation and the requirements that $S^{(a)}(q,\omega)=M^{(a)}(q,\omega)D(q,\omega)$ must produce the correct infrared exponent at $q=\pi$,[9,10] the correct q dependence of the known first frequency moment,[7,11] and, via sum rule, the correct value for the direct susceptibility.[4] The resulting (approximate) expression,[12]

$$S^{(a)}(q,\omega)=\frac{\Theta(\omega-\omega_L(q))\Theta(\omega_U(q)-\omega)}{\sqrt{\omega^2-\omega_L^2(q)}}, \qquad (2.2)$$

for the two-spinon dynamic structure factor has been widely used for the interpretation of inelastic neutron scattering measurements on a number of quasi-1D antiferromagnets at low temperature[6] and for comparisons with the results of various computational studies.[13,14]

It is interesting to note in this context that the exact dynamic structure factor $S(q,\omega)$ of the Haldane-Shastry model has a structure very similar to Eq. (2.2).[15] In that model, as in the XX model, all the spectral weight of $S(q,\omega)$ is carried by the two-spinon excitations.

A detailed assessment of the merits and limitations of the result (2.2) has become possible only recently through a remarkable new development. By approaches based on the concept of infinite-dimensional symmetries which had been developed in the context quantum groups[16] Bougourzi, Couture, and Kacir[17] were able to derive the exact expression for the two-spinon transition-rate function in the form[18]

$$M(q,\omega)=\frac{1}{2}e^{-I(t)}, \qquad (2.3)$$

where $t=2(\beta_1-\beta_2)/\pi$ and

$$I(t)=\int_0^\infty dx\frac{\cosh(2x)\cos(xt)-1}{x\sinh(2x)\cosh x}e^x, \qquad (2.4)$$

$$\omega=\frac{\pi}{2\cosh\beta_1}+\frac{\pi}{2\cosh\beta_2}, \qquad (2.5a)$$

$$q=-\cot^{-1}(\sinh\beta_1)-\cot^{-1}(\sinh\beta_2). \qquad (2.5b)$$

By solving Eqs. (2.5) we can express the auxiliary variable t as a function of the two physical variables q,ω:

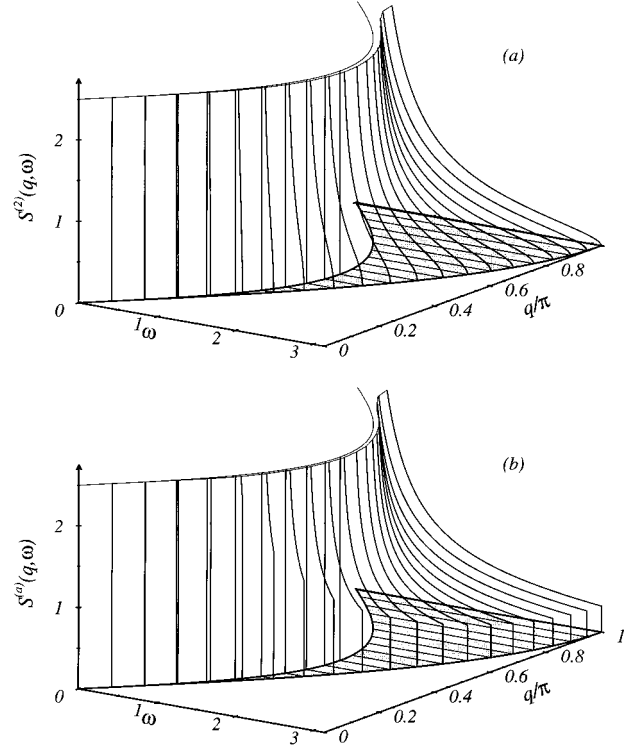$$t=\frac{4}{\pi}\cosh^{-1}\sqrt{\frac{\omega_U^2(q)-\omega_L^2(q)}{\omega^2-\omega_L^2(q)}}. \qquad (2.6)$$

FIG. 1. (a) Exact and (b) approximate two-spinon dynamic structure factor. Both expressions are nonzero only in the shaded region of the (q,ω) plane bounded by $\omega_L(q)$ and $\omega_U(q)$.

For the numerical evaluation of Eq. (2.3) we separate the singular part from the integral (2.4):

$$2I(t)=-I_0-\ln\left(t\sinh^2\frac{\pi t}{4}\right)-h(t), \qquad (2.7)$$

where

$$h(t)=\text{Ci}(t)+f_1(t)-f_2(t), \qquad (2.8a)$$

$$f_1(t)=\int_1^\infty\frac{dx}{x}\frac{\cos(xt)}{\cosh^2 x}, \quad f_2(t)=\int_0^1\frac{dx}{x}\frac{\cos(xt)}{\coth^2 x}, \qquad (2.8b)$$

$$I_0=\gamma+f_1(0)-f_2(0)=0.367\ 710\ 3\dots. \qquad (2.8c)$$

A series expansion of $s(t)\equiv[\ln t+I_0-h(t)]/2$,

$$s(t)=\int_0^\infty dx\frac{\sin^2(xt/2)}{x\cosh^2 x}=\sum_{m=1}^\infty(-1)^m m\ln\left(1+\frac{t^2}{4m^2}\right),$$

$$C\equiv e^{I_0}/2=0.722\ 21\dots, \qquad (2.9)$$

brings Eq. (2.3) with t from Eq. (2.6) into closed form:

$$M(q,\omega)=Ct\sinh\left(\frac{\pi t}{4}\right)\prod_{m=1}^\infty\frac{\{1+[t/(4m-2)]^2\}^{2m-1}}{\{1+[t/4m]^2\}^{2m}}.$$

The exact two-spinon part of $S(q,\omega)$, i.e., the function (1.7) with the density of states (1.5) and the transition-rate function (2.3) evaluated numerically via Eq. (2.7) with Eq. (2.6) is plotted in Fig. 1(a). For comparison, the approximate result (2.2) is shown in Fig. 1(b). The two results look very

similar, yet there are subtle differences, which may not matter for most experimental comparisons but are important for comparisons with other theoretical results. Both expressions diverge at the lower spectral boundary $\omega_L(q)$. At the upper boundary $\omega_U(q)$, $S^{(a)}(q,\omega)$ has a discontinuity, whereas $S^{(2)}(q,\omega)$ approaches zero continuously over a rounded shoulder. The structure of the exact transition-rate function (2.3) lends itself naturally to be factorized into the approximate function (2.1) and a correction which accounts for the modified singularities at the boundaries of the two-spinon continuum:

$$M(q,\omega)=M^{(a)}(q,\omega)\sqrt{Ct/2}\,e^{h(t)/2}. \tag{2.10}$$

III. SINGULARITIES AT $\omega_L(q)$ AND $\omega_U(q)$

What is the precise nature of the leading singularity in the transition-rate function $M(q,\omega)$ and in the two-spinon dynamic structure factor $S^{(2)}(q,\omega)$ at the spectral boundaries $\omega_U(q)$ and $\omega_L(q)$, and how do these singularities compare with those of the approximate results $S^{(a)}(q,\omega)$ and $M^{(a)}(q,\omega)$? The answer is obtained by inserting Eq. (2.7) into Eq. (2.3), evaluating the leading term for $t\to0$ and $t\to\infty$, respectively, and inserting Eq. (2.6) expanded accordingly.

At $\omega_U(q)$ the transition-rate function is thus found to approach zero linearly,

$$M(q,\omega)\overset{\omega\to\omega_U}{\to}\frac{8C}{\pi}\frac{\omega_U(q)}{\omega_U^2(q)-\omega_L^2(q)}[\omega_U(q)-\omega], \tag{3.1}$$

which implies that the two-spinon dynamic structure factor vanishes in a square-root cusp:

$$S^{(2)}(q,\omega)\overset{\omega\to\omega_U}{\to}\frac{8C}{\pi}\frac{\sqrt{2\omega_U(q)}}{\omega_U^2(q)-\omega_L^2(q)}\sqrt{\omega_U(q)-\omega}. \tag{3.2}$$

$M^{(a)}(q,\omega)$ vanishes more slowly, $\sim[\omega_U(q)-\omega]^{1/2}$, implying that $S^{(a)}(q,\omega)$ drops to zero abruptly.

At $\omega_L(q)$ we find a square-root divergence (for $q\neq\pi$) in both the exact and the approximate transition-rate functions, but in the former this power-law singularity is accompanied by a logarithmic correction:

$$M(q,\omega)\overset{\omega\to\omega_L}{\to}\frac{\sqrt{C/2}}{\pi}\sqrt{\frac{\omega_U^2(q)-\omega_L^2(q)}{\omega_L(q)}}\frac{1}{\sqrt{\omega-\omega_L(q)}}$$
$$\times\sqrt{\ln\frac{1}{\omega-\omega_L(q)}}. \tag{3.3}$$

Since the two-spinon density of states is a step function near $\omega_L(q)$, only the prefactor changes in $S^{(2)}(q,\omega)$:

$$S^{(2)}(q,\omega)\overset{\omega\to\omega_L}{\to}\frac{M(q,\omega)}{\sqrt{\omega^2(q)-\omega_L^2(q)}}. \tag{3.4}$$

For $q\to\pi$ the singularity at $\omega_L(q)$ turns into a much stronger infrared singularity:

$$M(\pi,\omega)\overset{\omega\to0}{\to}\sqrt{2\pi C}\frac{1}{\omega}\sqrt{\ln\frac{1}{\omega}}, \tag{3.5}$$

$$S^{(2)}(\pi,\omega)\overset{\omega\to0}{\to}\sqrt{\frac{2C}{\pi}}\frac{1}{\omega}\sqrt{\ln\frac{1}{\omega}}. \tag{3.6}$$

IV. SPIN AUTOCORRELATION FUNCTION

A quantity of some interest in various experimental and theoretical contexts is the frequency-dependent spin autocorrelation function

$$\Phi(\omega)\equiv\int_{-\infty}^{+\infty}dt\,e^{-i\omega t}\langle S_l^z(t)S_l^z\rangle. \tag{4.1}$$

The two-spinon contribution to $\Phi(\omega)$,

$$\Phi^{(2)}(\omega)\equiv\frac{1}{\pi}\int_0^\pi dq\,S^{(2)}(q,\omega), \tag{4.2}$$

is a piecewise smooth function over the range of two-spinon energies $0<\omega<\pi$ and has singularities at $\omega=0,\ \pi/2,\ \pi$. The approximate two-spinon autocorrelation function inferred from Eq. (2.2) can be evaluated in terms of elliptic integrals. It has a step discontinuity at $\omega=0$,

$$\Phi^{(a)}(\omega)\overset{\omega\to0}{\to}\frac{1}{\pi}+O(\omega), \tag{4.3}$$

a logarithmic divergence at $\omega=\pi/2$,

$$\Phi^{(a)}(\omega)\overset{\omega\to\pi/2}{\to}\propto\ln\frac{1}{|\pi/2-\omega|}, \tag{4.4}$$

and a square-root cusp at $\omega=\pi$,

$$\Phi^{(a)}(\omega)\overset{\omega\to\pi}{\to}\propto\sqrt{\pi-\omega}. \tag{4.5}$$

The exact two-spinon expression has logarithmic divergences at $\omega=0,\ \pi/2$, and a linear cusp at $\omega=\pi$:

$$\Phi^{(2)}(\omega)\overset{\omega\to0}{\to}\propto\ln\frac{1}{\omega}, \tag{4.6}$$

$$\Phi^{(2)}(\omega)\overset{\omega\to\pi/2}{\to}\propto\left(\ln\frac{1}{|\pi/2-\omega|}\right)^{3/2}, \tag{4.7}$$

$$\Phi^{(2)}(\omega)\overset{\omega\to\pi}{\to}\propto(\pi-\omega). \tag{4.8}$$

The functions $\Phi^{(2)}(\omega)$ and $\Phi^{(a)}(\omega)$ are plotted in Fig. 2.

V. FINITE-CHAIN MATRIX ELEMENTS

To what extent and accuracy can the spectral-weight distribution of $S(q,\omega)$ be reconstructed from Eq. (1.6) on the basis of finite-chain data for excitation energies ω_λ and transition rates M_λ? In a generic situation, the chances for success may be remote. Convergence of the finite-N data for Eq. (1.6) toward the infinite-N spectral density may only exist in an average sense, such as can be realized, at least in principle, by a histogram representation of Eq. (1.6), but hardly in practice given the very coarse-grained spectral-weight dis-
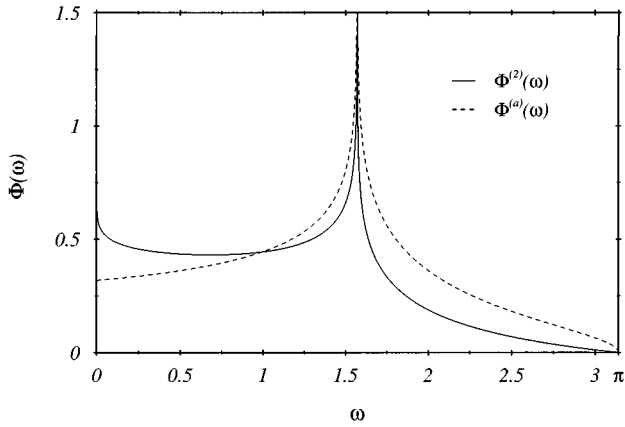
FIG. 2. Two-spinon part of the frequency-dependent spin auto-correlation function. The solid line represents the exact result $\Phi^{(2)}(\omega)$ and the dashed line the approximate result $\Phi^a(\omega)$.

FIG. 3. Two-spinon transition-rate function at $q=\pi$. The solid line represents the exact result $M(q,\omega)$ and the dashed line the approximate result $M^{(a)}(q,\omega)$. Also shown are scaled finite-chain transition rates NM_λ for all two-spinon excitations at $q=\pi$ of systems with $N=6,8,\ldots,16,28$ spins, and for lowest two-spinon excitations also of systems with $N=18,20,\ldots,26$. The low-frequency and high-frequency parts are shown again in the insets with transformed scales on both axes.

tribution even in the largest systems that can be handled computationally.

Among the ever growing collection of Bethe ansatz solvable models, there exist numerous situations where the spectral density of interest is dominated by a specific class of excitations that can be identified in terms of Bethe quantum numbers. When the dynamically dominant class of excitations consists of a two-parameter continuum, as is frequently the case, the task of reconstructing that spectral density from finite-N data with reasonable accuracy may be perfectly within the reach of state-of-the-art computational applications.

In the case at hand, the two-spinon excitation energies ω_λ can be evaluated for finite chains over a wide range of N and then again for infinite N, all via Bethe ansatz. The finite-N transition rates M_λ can be evaluated directly from the Bethe ansatz wave function for the ground state and the two-spinon states up to $N=16$ and indirectly from the finite-N ground-state wave function via the recursion method[14] up to $N=28$.

The crucial point for the reconstruction of the two-spinon part of the dynamic structure factor $S(q,\omega)$ is that it factorizes into two smooth functions: the density of states $D(q,\omega)$, which can be determined exactly via Bethe ansatz, and the transition rate function $M(q,\omega)$, toward which the finite-N transition rates seem to converge in the following sense: pick any sequence of finite-N two-spinon states with energies $\omega_\lambda(N)$ and wave numbers $q_\lambda(N)$ converging toward (q,ω) as $N\to\infty$. Then the associated scaled transition rates NM_λ converge toward the exact transition rate function $M(q,\omega)$.

In the main plot of Fig. 3 we show the transition rate functions $M(\pi,\omega)$ (exact, solid line) and $M^{(a)}(\pi,\omega)$ (approximate, dashed line) along with scaled finite-N transition rates NM_λ for $N=6,8,\ldots,28$. The downward deviation of $M^{(a)}(\pi,\omega)$ from $M(\pi,\omega)$ at low frequencies is due to the lacking logarithmic corrections in the infrared divergence and the upward deviation at high frequencies due to the different cusp singularity at $\omega_U(\pi)$.

All finite-N data points fall close to the solid line. Their deviations from that line have an irregular appearance at first sight. This is attributable to the fact that an increasing num-
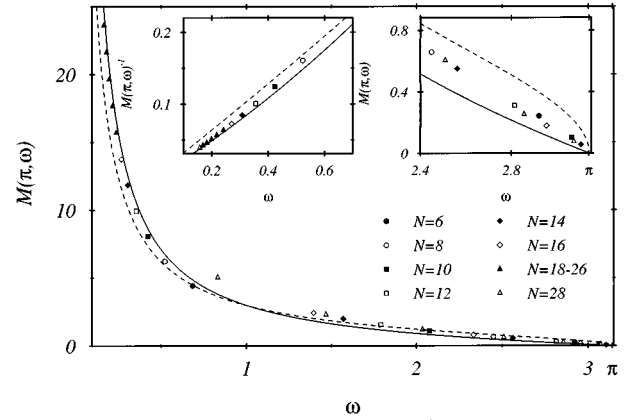
ber of spectral contributions from systems with increasing N are distributed over a fixed frequency interval. However, when we focus on the lowest-lying excitation, for example, we see that the data points move away from the dashed line toward the solid line. The uniform convergence of this particular sequence of data points is best observable in the representation of the inset on the left of Fig. 3.

The region near $\omega_U(\pi)$ is shown magnified in the inset on the right. Here the finite-N data converge in a much more complicated pattern. Nevertheless, the trend is clearly toward the linear behavior of the solid line and away from the square-root behavior of the dashed line.

The corresponding results for $q=\pi/2$ are depicted in Fig. 4. Here the highest two-spinon excitation for $N=28$, which we were unable to compute with sufficient accuracy via the
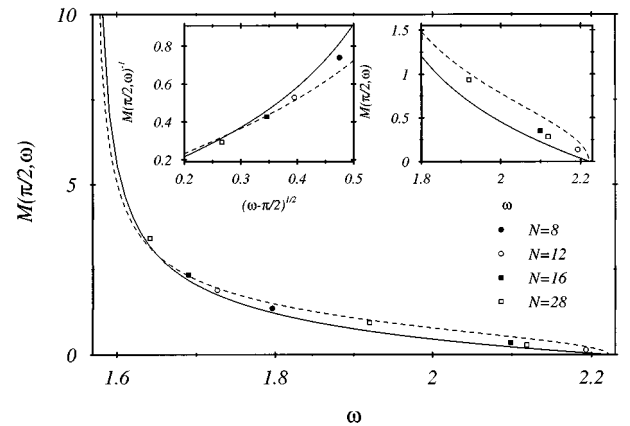

FIG. 4. Two-spinon transition-rate function at $q=\pi/2$. The solid line represents the exact result $M(q,\omega)$ and the dashed line the approximate result $M^{(a)}(q,\omega)$. Also shown are scaled finite-chain transition rates NM_λ for all two-spinon excitations at $q=\pi$ of systems with $N=8,12,16,28$ spins. The low-frequency and high-frequency parts are shown again in the insets with transformed scales on both axes.

recursion method, is not included. Even with the few finite-chain data points available in this case, the finite-size scaling behavior of the transition rates M_λ and their convergence toward the exact transition-rate function is again convincingly determined.

VI. SUM RULES

How important is the two-spinon contribution to $S(q,\omega)$ in relation to that of other excited states? The key to the answer is provided by sum rules, such as the first frequency moment, which is known for all q,

$$K_1(q) \equiv \int_0^\infty \frac{d\omega}{2\pi} \omega S(q,\omega) = \frac{2E_G}{3N}(1-\cos q), \quad (6.1)$$

and where $E_G = -N(\ln 2 - 1/4)$ is the ground-state energy,[2] or the susceptibility,

$$\chi(q) \equiv \frac{1}{\pi} \int_0^\infty \frac{d\omega}{\omega} S(q,\omega), \quad (6.2)$$

which is known for $q=0$ only,[4] $\chi(0) = 1/\pi^2$, or the integrated intensity (static structure factor),

$$I(q) \equiv \int_0^\infty \frac{d\omega}{2\pi} S(q,\omega), \quad (6.3)$$

of which we know the grand total:

$$I_T = \frac{1}{\pi} \int_0^\pi dq I(q) = \langle (S_l^z)^2 \rangle = \frac{1}{4}. \quad (6.4)$$

The exact two-spinon contribution to the nth frequency moment of $S(q,\omega)$,

$$K_n(q) \equiv \int_0^\infty \frac{d\omega}{2\pi} \omega^n S(q,\omega), \quad (6.5)$$

as obtained from Eq. (1.7) with Eqs. (1.5) and (2.3) can be brought into the form

$$K_n^{(2)}(q) = \frac{2C}{\pi^3} [\omega_U(q)]^{n+1} k_n(q), \quad (6.6)$$

where

$$k_n(q) = \int_0^\infty dx \frac{x \sinh x}{\cosh^2 x} \left(1 - \sin^2 \frac{q}{2} \tanh^2 x\right)^{(n-1)/2} e^{-s(4x/\pi)}. \quad (6.7)$$

For $n = 2m+1 = 1,3,\ldots$ this expression reduces to a polynomial in $\cos q$,

$$K_{2m+1}^{(2)}(q) = \frac{C}{\pi} \left(\frac{\pi^2}{2}\right)^m \sum_{l=0}^m \binom{m}{l} \frac{(-1)^l}{2^l} \kappa_l (1-\cos q)^{m+1+l}, \quad (6.8a)$$

$$\kappa_l \equiv \int_0^\infty dx \frac{x(\tanh x)^{2l+1}}{\cosh x} e^{-s(4x/\pi)}. \quad (6.8b)$$

The exact sum rules for $K_{2m+1}(q)$ were shown to have precisely this general structure,[19,20] which, incidentally, is also reproduced by the frequency moments $K_{2m+1}^{(a)}(q)$ of

$S^{(a)}(q,\omega)$. However, the exact coefficients of the polynomial are only known for $m=0$. Comparison of

$$K_1^{(2)}(q) = \frac{C}{\pi} \kappa_0(1-\cos q), \quad \kappa_0 = 0.9163\ldots, \quad (6.9)$$

with Eq. (6.1) provides one way of measuring the relative spectral weight of the two-spinon excitations:

$$\frac{K_1^{(2)}(q)}{K_1(q)} = 0.7130\ldots, \quad (6.10)$$

A somewhat larger share of spectral weight, $K_1^{(a)}(q)/K_1(q) = 0.8462\ldots$, is accounted for by $S^{(a)}(q,\omega)$.

A different way of measuring the relative two-spinon spectral weight is provided by the static structure factor (6.3). Here, the missing spectral weight of higher-lying excitations is weighted less heavily. The exact two-spinon static structure factor $I^{(2)}(q) = K_0^{(2)}(q)$ taken from Eq. (6.6) and integrated over q yields the total two-spinon intensity

$$I_T^{(2)} = \frac{4C}{\pi^3} \int_0^\infty dx \frac{x^2}{\cosh x} e^{-s(4x/\pi)} \simeq 0.7289 I_T. \quad (6.11)$$

The total intensity of $S^{(a)}(q,\omega)$ is[7] $I_T^{(a)} \simeq 0.7424 I_T$.

The observation that $S^{(a)}(q,\omega)$ overestimates the total two-spinon intensity by a smaller fraction, $I_T^{(a)}/I_T^{(2)} \simeq 1.0185$, than the first frequency moment of the two-spinon spectral weight, $K_1^{(a)}(q)/K_1^{(2)}(q) \simeq 1.1868$, is consistent with the observation that it predicts too much spectral weight near $\omega_U(q)$ and too little near $\omega_L(q)$.

At small q, where the two-spinon continuum is very narrow, all frequency moments of $S^{(2)}(q,\omega)$ and $S^{(a)}(q,\omega)$ have exactly the same ratio

$$\frac{K_n^{(a)}(q)}{K_n^{(2)}(q)} \xrightarrow{q \to 0} \frac{4C}{\pi} \kappa_0 = 0.8426\ldots. \quad (6.12)$$

The implications of the frequency moments $K_0^{(2)}(q)$ and $K_{-1}^{(2)}(q)$ for the singularities of the static structure factor and the static susceptibility, respectively, are as follows. Given the exact asymptotic finite-size gap of the lowest two-spinon excitation at $q = \pi$,[21]

$$\omega_1 \xrightarrow{N \to \infty} \frac{\alpha}{N}, \quad \alpha = \frac{\pi^2}{2}, \quad (6.13)$$

and the exact infrared divergence (3.6) of $S^{(2)}(q,\omega)$, it is possible to determine, under standard scaling assumptions, the leading N dependence of the integrated intensity at $q = \pi$,

$$I(\pi,N) \xrightarrow{N \to \infty} \frac{m_0}{2\pi} (\ln N)^{3/2} \quad (6.14)$$

with $m_0 = \sqrt{2C/\pi}$. The exact coefficient, $m_0/2\pi = 0.1079\ldots$, is significantly higher than the value 0.090 52 predicted in a recent DMRG study.[22] The leading singularity of the integrated intensity for $N = \infty, q \to \pi$ is then predicted to be of the form
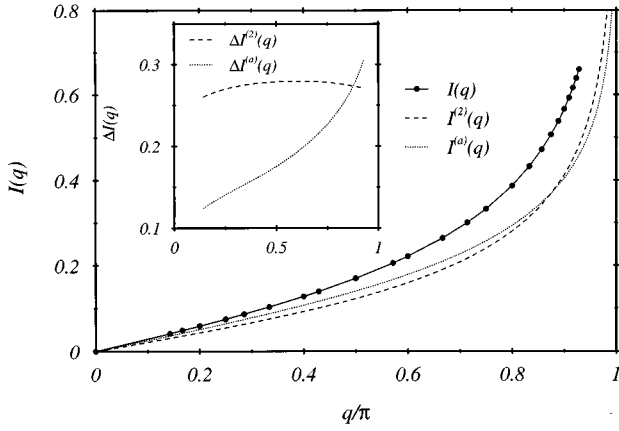
FIG. 5. Integrated intensities (6.3) in comparison: $I(q)$ is represented by finite-N data for $N=6,8,\ldots,28$. $I^{(2)}(q)$ is the exact two-spinon result. $I^{(a)}(q)$ is the approximate result (7.1). The inset shows $\Delta I^{(2)}(q)=1-I^{(2)}(q)/I(q)$ and $\Delta I^{(a)}(q)=1-I^{(a)}(q)/I(q)$.

$$I^{(2)}(q) \overset{q\to\pi}{\to} \frac{m_0}{2\pi}\left[-\ln\left(1-\frac{q}{\pi}\right)\right]^{3/2}, \qquad (6.15)$$

which is consistent with the exactly known leading asymptotic term of the static spin correlation function[23] $\langle S_l^z S_{l+n}^z\rangle \sim (-1)^n n^{-1}(\ln n)^{1/2}/n$.

The corresponding leading terms for the static susceptibility read

$$\chi(\pi,N) \overset{N\to\infty}{\to} \frac{m_0}{\pi\alpha} N\sqrt{N}, \qquad (6.16)$$

$$\chi^{(2)}(q) \overset{q\to\pi}{\to} \propto \frac{\sqrt{-\ln(\pi-q)}}{\pi-q}. \qquad (6.17)$$

VII. SIGNIFICANCE OF NON-TWO-SPINON PART OF $S(q,\omega)$

Where in (q,ω) space is the remaining spectral weight, and how does it affect various quantities that can be derived from the dynamic structure factor? In answer to these questions, we investigate here the effects of the non-two-spinon excitations on four quantities which are related to $S(q,\omega)$ and which can be computed with high precision from finite-N data for the ground-state wave function.

A. Integrated intensity

The integrated intensity of $S(q,\omega)$, i.e., the static spin structure factor (6.3) has been determined with high precision for wave numbers $q\leqslant 13\pi/14$ from finite-N data of cyclic chains with $N\leqslant 28$ sites.[24] This result is plotted in Fig. 5 for comparison with the exact two-spinon integrated intensity $I^{(2)}(q)$ calculated from $S^{(2)}(q,\omega)$ via (6.3) and the integrated intensity[7]

$$I^{(a)}(q) = \frac{1}{2\pi}\ln\frac{1+\sin(q/2)}{\cos(q/2)} \qquad (7.1)$$

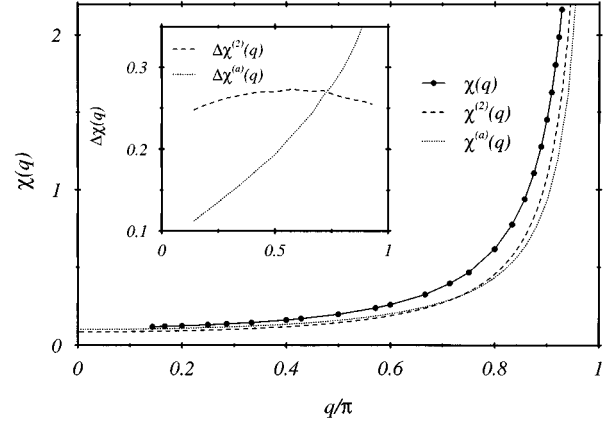obtained from the approximate result $S^{(a)}(q,\omega)$.

FIG. 6. The q dependent susceptibilty (6.2) in comparison: $\chi(q)$ is represented by finite-N data for $N=6,8,\ldots,28$. $\chi^{(2)}(q)$ is the exact two-spinon result. $\chi^{(a)}(q)$ is the approximate result (7.2). The inset shows the relative non-two-spinon integrated intensity $\Delta\chi^{(2)}(q)=1-\chi^{(2)}(q)/\chi(q)$ and $\Delta\chi^{(a)}(q)=1-\chi^{(a)}(q)/\chi(q)$.

The finite-N data indicate that $I(q)$ increases linearly from zero for small q and diverges logarithmically at $q=\pi$. The initial rise of the finite-N data, $I(q)\to 0.271q/\pi$,[19] is significantly steeper than that of the two-spinon contribution, $I^{(2)}(q)\to 0.210q/\pi$ and that of the approximate result, $I^{(a)}(q)\to 0.25q/\pi$. Hence the integrated intensity of the non-two-spinon part of $S(q,\omega)$ increases linearly in q too.

The function $I^{(a)}(q)$ approximates the two-spinon integrated intensity $I^{(2)}(q)$ quite well for $q/\pi\lesssim 0.6$. At larger q, this is no longer the case. The divergence predicted by expression (7.1), $I^{(a)}\sim -\ln(1-q/\pi)$, is weaker than the divergence (6.15) of the exact two-spinon result. The inset of Fig. 5 shows the relative non-two-spinon integrated intensity, $\Delta I^{(2)}(q)=1-I^{(2)}(q)/I(q)$, and the relative deviation, $\Delta I^{(a)}(q)=1-I^{(a)}(q)/I(q)$, of the approximate result (7.1). If it can be assumed that the leading singularity of $I(q)$ at $q=\pi$ is produced entirely by the two-spinon part of $S(q,\omega)$, then the function $\Delta I^{(2)}(q)$ must approach zero as $q\to\pi$. The dashed line in the inset does not rule out that this assumption is correct.

It is interesting to compare these results with the exact integrated intensity of the Haldane-Shastry model,[15] $I^{(HS)}(q)=-(1/4)\ln(1-q/\pi)$, where non-two-spinon excitations have zero spectral weight in $S(q,\omega)$. It turns out that for $q\lesssim 13\pi/14$, $I^{(HS)}(q)$ is a better approximation of $I(q)$ than $I^{(2)}(q)$ is.[24]

B. Susceptibility

The q dependent susceptibility at $T=0$ is related to $S(q,\omega)$ via the sum rule (6.2). This quantity, which has been determined with considerable accuracy from finite-N data, is plotted in Fig. 6 for comparison with the exact two-spinon susceptibility $\chi^{(2)}(q)$ calculated from $S^{(2)}(q,\omega)$ via Eq. (6.2) and the approximate result[7]

$$\chi^{(a)}(q) = \frac{1}{\pi^2}\frac{q}{\sin q} \qquad (7.2)$$

inferred from Eq. (2.2).

The normalization of $S^{(a)}(q,\omega)$ was chosen such that the exact value of the direct susceptibilty,[4] $\chi(0)=1/\pi^2$, is correctly reproduced. With increasing q, $\chi^{(a)}(q)$ deviates in a downward direction from $\chi(q)$. Its divergence at $q=\pi,\chi^{(a)}(q)\sim(\pi-q)^{-1}$, is slightly weaker than the divergence (6.17) of the exact two-spinon susceptibilty.

The contribution of the non-two-spinon spectral weight of $S(q,\omega)$ to $\chi(q)$ in the limit $q\to0$ is small as indicated by the result $\pi^2\chi^{(2)}(0)=0.8426\ldots$. The relative non-two-spinon contribution to the susceptibility, $\Delta\chi^{(2)}(q)=1-\chi^{(2)}(q)/\chi(q)$, stays smaller than the relative non-two-spinon integrated intensity $\Delta I^{(2)}(q)$ (see inset). This indicates that the non-two-spinon spectral weight is located predominatly above the two-spinon continuum.

C. Frequency moments

Yet a different way to assess the non-two-spinon part of $S(q,\omega)$ employs the frequency moments (6.5) which are related, via sum rules,[20] to short-range multispin correlations in the ground state. For $n=1$ we know the exact results (6.1). For $n=2,3,4,5$ high-precision results have been calculated from finite-N data for the associated ground-state expectation values.[19] The moments $K_n^{(2)}(q)$ of the exact two-spinon dynamic structure factor $S^{(2)}(q,\omega)$ have been determined in Eq. (6.6) and the moments $K_n^{(a)}(q)$ of $S^{(a)}(q,\omega)$ in Ref. 20.

For $n=1$, both $K_1^{(2)}(q)$ and $K_1^{(a)}(q)$ reproduce the q dependence of the exact sum rule (6.1) correctly, but the prefactors are smaller,

$$\frac{K_1^{(2)}(q)}{K_1(q)}=0.7130\ldots, \quad \frac{K_1^{(a)}(q)}{K_1(q)}=0.8462\ldots, \quad (7.3)$$

which again reflects the missing spectral weight of the non-two-spinon excitations. The q dependence of the moment ratios

$$R_n(q)\equiv\frac{K_n(q)}{K_1(q)} \quad \text{for } n=2,3,4,5, \quad (7.4)$$

of the full dynamic structure factor as inferred from finite-N data are shown in Fig. 7 along with the corresponding moment ratios $R_n^{(2)}(q)$ of $S^{(2)}(q,\omega)$ and the moment ratios $R_n^{(a)}(q)$ of $S^{(a)}(q,\omega)$. The most striking observation is that $R_n(q)$ approaches a nonzero value as $q\to0$, whereas the exact and the approximate two-spinon moment ratios both go to zero: $R_n^{(2)}(q)\sim R_n^{(a)}(q)\sim q^{n-1}$. This means that for long wavelengths the frequency moments $K_n(q)$, $n\geq2$, are dominated by non-two-spinon excitations, which are necessarily located above the narrow two-spinon band. In other words, the two-spinon dynamic structure factor $S^{(2)}(q,\omega)$ does not contribute to the leading $O(q^2)$ term of $K_n(q)$ for $n\geq2$.

At larger wave numbers, the impact of the non-two-spinon excitations on the moment ratios is more modest but still significant. Here the deviation of $R_n^{(2)}(q)$ from $R_n(q)$ is almost q independent, and it grows with increasing n. This again indicates that the non-two-spinon spectral weight comes for the most part from higher frequencies than the two-spinon spectral weight.
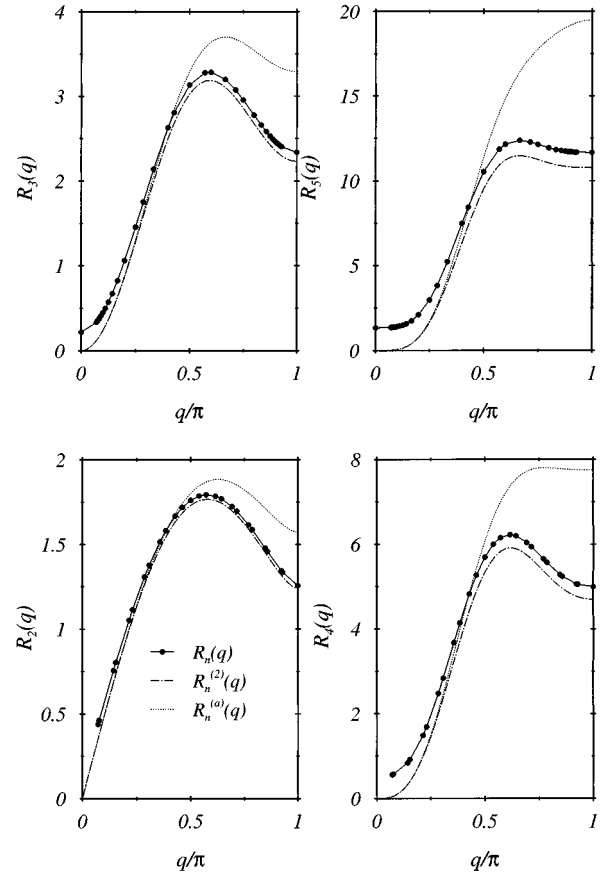

FIG. 7. Ratios of frequency moments (7.4). For $n=2,3,4,5$, the $R_n(q)$ represent finite-N data for $N=6,\ldots,28$. The $R_n^{(2)}(q)$ are exact two-spinon results and the $R_n^{(a)}(q)$ are the moment ratios for Eq. (2.2).

The moment ratios $R_n^{(a)}(q)$ agree very well with $R_n^{(2)}(q)$ at small q, but then deviate upwardly. For $q\gtrsim\pi/3$, they rise even above the ratios $R_n(q)$. This discrepancy, which becomes more conspicuous with increasing n, again reflects the fact that $S^{(a)}(q,\omega)$ underestimates the spectral weight near the lower continuum boundary $\omega_L(q)$ and overestimates the spectral weight near the upper boundary $\omega_U(q)$.[19]

D. Euclidian time representation

We can study the significance of the non-two-spinon excitations in a dynamical quantity by the same kind of comparison if we consider the Laplace transform of the dynamic structure factor,[14]

$$\widetilde{S}(q,\tau)\equiv\int_0^\infty\frac{d\omega}{2\pi}e^{-\omega\tau}S(q,\omega). \quad (7.5)$$

This quantity can be interpreted as a Euclidian time representation of $S(q,\omega)$. For $\tau=0$, it is the integrated intensity (6.3). From finite-N data for $S(q,\omega)$ as obtained via the recursion method for systems with $N\leq28$ sites,[14] this quantity can be accurately extrapolated to $N\to\infty$ if $q\neq\pi$. For the graphical representation, it is convenient to plot the function

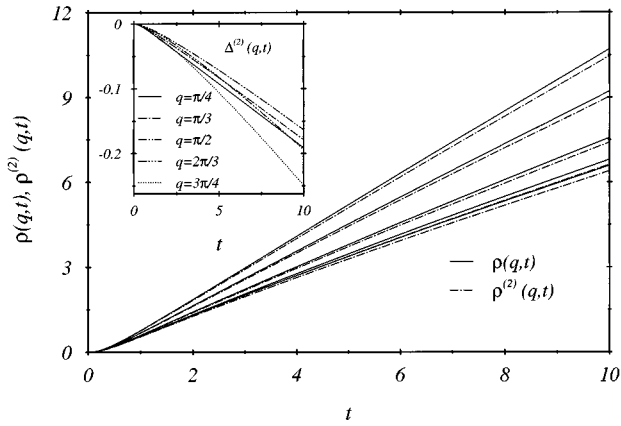FIG. 8. The function (7.6) for $q = \pi/4$, $\pi/3$, $\pi/2$, $2\pi/3$, $3\pi/4$ (bottom to top). The solid lines represent extrapolated finite-N data and the dashed lines the exact two-spinon-part of that function. The inset shows the non-two-spinon part $\Delta^{(2)}(q,t)$ of the same function.

$$\rho(q,t) \equiv \frac{\widetilde{S}(q,0)}{\widetilde{S}(q,\tau)} - 1, \quad t = \sqrt{\omega_L(q)\tau} \exp[\,\omega_L(q)\tau\,],$$
$$(7.6)$$

which was used for the finite-N extrapolation, instead of $\widetilde{S}(q,\tau)$ itself. The resulting curves, shown as solid lines in Fig. 8 for several q values, rise from zero with zero initial slope and then become almost linear in t with a q dependent slope.

If the threshold singularity were a square-root divergence as predicted by Eq. (2.2), then the asymptotic growth of $\rho(q,t)$ would be exactly linear. The logarithmic correction in the exact two-spinon threshold singularity (3.4), however, leads to a slight modification of the asymptotic growth of $\rho(q,t)$,

$$\rho^{(2)}(q,t) \overset{t \to \infty}{\to} \propto \frac{t}{\ln\ln t}.\qquad(7.7)$$

The dashed lines in Fig. 8 show the function $\rho^{(2)}(q,t)$ as inferred from the exact two-spinon dynamic structure factor. The discrepancies are fairly small over the range of t shown. The deviation $\Delta^{(2)}(q,t) = \rho^{(2)}(q,t) - \rho(q,t)$ is shown in the inset. Not surprisingly, the function $\rho^{(a)}(q,t)$ inferred from Eq. (2.2) deviates more strongly from $\rho(q,t)$. This comparison was already made in Ref. 14.

ACKNOWLEDGMENTS

[1] H. Bethe, Z. Phys. **71**, 205 (1931).

[2] L. Hulthén, Arkiv Mat. Astron. Fys. A11 **26**, 1 (1938).

[3] J. des Cloizeaux and J.J. Pearson, Phys. Rev. **128**, 2131 (1962).

[4] R.B. Griffiths, Phys. Rev. **133**, A768 (1964); C.N. Yang and C.P. Yang, *ibid.* **150**, 321 (1966); **150**, 327 (1966); **151**, 258 (1966).

[5] M. Gaudin, Phys. Rev. Lett. **26**, 1301 (1971); M. Takahashi, Prog. Theor. Phys. **46**, 401 (1971).

[6] S.E. Nagler *et al.*, Phys. Rev. B **44**, 12 361 (1991); D.A. Tennant, T.G. Perring, R.A. Cowley, and S.E. Nagler, Phys. Rev. Lett. **70**, 4003 (1993); D.C. Dender *et al.*, Phys. Rev. B **53**, 2583 (1996).

[7] G. Müller, H. Thomas, H. Beck, and J.C. Bonner, Phys. Rev. B **24**, 1429 (1981).

[8] T. Niemeijer, Physica **36**, 377 (1966); S. Katsura, T. Horiguchi, and M. Suzuki, *ibid.* **46**, 67 (1970).

[9] A. Luther and I. Peschel, Phys. Rev. B **12**, 3908 (1975).

[10] The logarithmic corrections to the $\sim\omega^{-1}$ singularity were not known at the time.

[11] P.C. Hohenberg and W.F. Brinkman, Phys. Rev. B **10**, 128 (1974).

[12] Alternative requirements considered in Ref. 8 yield prefactors in Eq. (2.2) which are slightly greater than one.

[13] S. Haas, J. Riera, and E. Dagotto, Phys. Rev. B **48**, 3281 (1993); K. Hallberg, *ibid.* **52**, R9827 (1995).

[14] A. Fledderjohann, M. Karbach, K.-H. Mütter, and P. Wielath, J. Phys.: Condens. Matter **7**, 8993 (1995).

[15] F.D.M. Haldane, Phys. Rev. Lett. **60**, 635 (1988); **60**, 1866; B.M. Shastry, *ibid.* **60**, 639 (1988); F.D.M. Haldane and M.R. Zirnbauer, *ibid.* **71**, 4055 (1993); J.C. Talstra and F.D.M. Haldane, Phys. Rev. B **50**, 6889 (1994).

[16] M. Jimbo and T. Miwa, *Algebraic Analysis of Solvable Lattice Models* (American Mathematical Society, Providence, 1995).

[17] A.H. Bougourzi, M. Couture, and M. Kacir, Phys. Rev. B **54**, R12 669 (1996).

[18] We have found and corrected a discrepancy in Chap. 10.4 of Ref. 16, which affects the constant prefactor in Eq. (2.3).

[19] A. Fledderjohann, M. Karbach, and K.-H. Mütter, Phys. Rev. B **53**, 11 543 (1996).

[20] G. Müller, Phys. Rev. B **26**, 1311 (1982).

[21] F. Woynarovich and H.-P. Eckle, J. Phys. A **20**, L97 (1987).

[22] K. Hallberg, P. Horsch, and G. Martínez, Phys. Rev. B **52**, R719 (1995).

[23] R.R.P. Singh, M.E. Fisher, and R. Shankar, Phys. Rev. B **39**, 2562 (1989).

[24] M. Karbach and K.-H. Mütter, Z. Phys. B **90**, 83 (1993); M. Karbach, K.-H. Mütter, and M. Schmidt, Phys. Rev. B **50**, 9281 (1994).